Extensive analysis of PCM-based heat sink with different fin arrangements under varying load conditions and variable aspect ratio

Nedumaran, Muthamil Selvan; Gnanasekaran, Nagarajan; Hooman, Kamel

DOI
10.1016/j.est.2023.108870

Publication date
2023

Document Version
Final published version

Published in
Journal of Energy Storage

Journal of Energy Storage 73 (2023) 108870

Contents lists available at ScienceDirect

Journal of Energy Storage

journal homepage: www.elsevier.com/locate/est

Research Papers

Extensive analysis of PCM-based heat sink with different fin arrangements under varying load conditions and variable aspect ratio

Muthamil Selvan Nedumaran [a], Nagarajan Gnanasekaran [a], Kamel Hooman [b,*]

[a] Dept. of Mechanical Engineering, National Institute of Technology Karnataka, Surathkal 575025, India
[b] Dept. of Process and Energy, Delft University of Technology, Netherlands

ARTICLE INFO

Keywords:
Phase change material
Pulsed power surge
Heat sink
Transient thermal response
Variable fin height
Melting
Solidification

ABSTRACT

The present study compares a modified variable height fin heat sink with the conventional constant height fin heat sink. The two heat sinks are filled with an equal volume of PCM (n-eicosane) and a fin volume fraction of 8 %. The experiments are performed for constant loads and also different power surge conditions. The pulsed heat loads are applied for two scenarios: 1. Constant load 4 W - power surge and constant load 4 W - power surge - 1800 s no-load condition, and 2. Power surge (50 s, 100 s, and 150 s) - no-load conditions of 1800 s. During experiments, the proposed variable height fin heat sinks possess better thermal performance for all load scenarios. Further, a 3D computational model is developed using ANSYS Fluent 19 to assess not only the effect of fin arrangement for different aspect ratios but also the impact of fin shape. The enclosure aspect ratio employed for the given study ranges from 0.3 to 0.8 for both the heat sinks. Regarding the fin structure in a heat sink, four types of fin shapes are adopted: square, circular, diamond, and triangular. The contour images of temperature and the liquid fraction are shown for the charging process. For the discharging process, the time required for the heat sinks to completely solidify the PCM is discussed. From the outcomes, variable height fin heat sinks provide enhanced melting/solidification for all the aspect ratios and fin shapes considered. As the aspect ratio increases, the time difference between the heat sink for the completion of the discharging cycle is reduced. Moreover, the triangular shaped fin shows a higher enhancement percentage of 2.29 % and 1.43 % during melting and 6.25 % and 12.5 % during solidification for both the heat sinks, respectively.

1. Introduction

Due to its advanced functionality, the growth in compact electronics has become an integral part of the current era. The miniaturization of electronics and the multi-tasking ability of these devices lead to overheating and failure. This oversight makes the device less efficient and unreliable. Hence, thermal management is crucial for designing and developing electronics to control the device at the desired operating temperature. Currently, conventional cooling methods are not effective enough. Therefore, high-performing electronic devices need efficient techniques to fulfill their cooling needs. The cooling methods in the current scenario are active and passive methods. Active cooling uses natural convection by placing the heat sink directly on the chip to extract heat. Here mostly, fins are attached to the surface of heat sinks to reduce the operating temperature.

Similarly, fans are placed near the heat sink in forced convection to increase the cooling efficiency. But the fans attached to the system increase the noise, size, and vibrations. By replacing the active method, the passive methods can lead to more reliable performance and longer device life. Inheriting PCM in passive cooling was found effective by various researchers [1–6]. The high heat of fusion and nearly isothermal during phase transition allows PCM to extract a large amount of heat from the source. However, their applications in thermal management are limited because of their low thermal conductivity. Materials with high thermal conductivity should be added to PCM for suitable electronic cooling. In past research, several enhancers, including foams [7–9], machined fins [10–12], nanoparticles [13–15], and heat pipes [16,17], are added to the PCM to improve their thermal conductivity. Among these fillers, fins were effective due to their simple structure and ease of manufacturing.

Several authors have reported the insertion of fins in PCM-based heat sinks for various applications. Mosaffa et al. [18] developed an analytical model for the shell and tube finned storage system for air-conditioned systems. They incorporated radial fins and compared the

* Corresponding author.
E-mail address: k.hooman@tudelft.nl (K. Hooman).

https://doi.org/10.1016/j.est.2023.108870
Received 13 June 2023; Received in revised form 14 August 2023; Accepted 29 August 2023
Available online 12 September 2023

cylindrical shell and rectangular storage enclosure. Due to conduction, the influence of fins is more during solidification than melting, and cylindrical storage possesses a faster solidification rate. Bouhal et al. [19] integrated a finned PCM setup into the passive solar building. Rectangular and triangular fin shapes were proposed, and the melting time was reduced by adding a rectangular fin shape than a triangular fin shape. They concluded that the fins added at the heat source improve the overall heat transfer. Different fin structures were employed by Elmaazouzi et al. [20], and their impact on the solar storage system was studied. The increase in fin thickness and decrease in fin number diminishes the thermal performance. The storage system with longitudinal fins reduces the charging time better than the system with hexagonal fins and circular fins. The PCM container is placed at the back of the PV panel by Khanna et al. [21] to increase its efficiency. The effect of fin spacing, fin length, and fin thickness is evaluated, and the best fin was found for the PV-PCM system. Sun et al. [22] investigated the influence of fin structure in battery thermal management systems. The proposed straight and arc fins could prolong the working time by 157 %, 189 %, and 238 % at ambient conditions of 20 °C, 30 °C, and 40 °C. The effect of honeycomb fin in a battery was evaluated by Liu et al. [23]. The optimal honeycomb fin maintains the battery temperature below 50 °C for a longer time, and the temperature is decreased by 23.3 % compared with other structure. For satellite application, Desai et al. [24], numerically investigated the effective fin configuration. The critical temperature is found less for the triangular prism geometry and it provides a superior thermal performance.

The researchers employed different configurations of fins to maximize the heat transfer performance. Miers and Marconnet [25] designed a composite heat sink with an iso grid and iso kite deltoid fins for electronic cooling. The package sizes for the investigation are 25 mm × 25 mm and 50 × 50 mm. The effect of fins is evaluated based on the time taken for the chip to attain critical temperature. The iso kite finned design achieves better results than the other packages. Also, a guideline for the selection of PCM was stated. Singh and Giri [26] experimentally compared the effect of fin numbers and fin volume fraction. The fins are arranged according to constant and dual fin heights by keeping the same fin numbers. The enhancers with a 9 % volumetric fraction yield superior performance. The dual height fins achieved a prolonged operational time than the constant height fins. The fully filled PCM heat sink extends the operating time longer than the partially filled system. Ali et al. [27] reviewed the influence of fin cross-sections in pin-fin configured heat sinks. Three geometries, triangular, rectangular, and circular pin fins, are considered for efficient cooling. Simultaneously, six different PCM with different properties are selected. The most effective configuration from the analysis is a triangular cross-section for cases with and without PCM. In the case of varying PCM in all heat sinks, RT-44 was found better to control the critical temperature. Desai et al. [28] introduced an inverted fin design for peak thermal control in an electronic device. The parameters of machined fins, such as the mass of fins, number of fins, shape, and cross-section of fins, are assorted. The peak temperature observed in the heat sinks is reduced by increasing the number of fins. Similarly, for prism fin and inverted fin, 20 % and 25 % mass of fins achieved the lowest peak temperature. The inverted fins attribute higher surface area and increase the heat-conducting pathways. Among the fin configurations, the inverted star fin attains a feasible response. In an enclosure, a double fin length arrangement was developed by Ji et al. [29]. The impact of unequal fin lengths with RT42 as PCM and heating with an input of constant temperature was investigated. The upper short fins and lower long fins significantly affect the melt fraction. An optimum of 0.11 fin-length ratio effectively saves up to 40.5 % of the melting time.

Akula and Balaji [30] examined the PCM-based heat sinks subjected to constant and pulsed power heat loads. The TCE configuration variation has a dominant effect during constant loads for a short period. Vertical square fins regulate the heater temperature when spiked loads are applied. The control of operating temperature in a heat sink vanishes once the PCM is completely melted in the heat sink. A cross-plate fin with eutectic alloy as PCM was tested by Yang et al. [31]. A power load of 80 W, 200 W, and 320 W is applied as heat input. $Bi_{31.6}In_{48.8}Sn_{19.6}$ (E-BiInSn), which is a low melting point metal, and octadecanol are used as PCM. Under high-load heating conditions, the liquid metal PCM exhibits excellent heat extraction compared to octadecanol. A cyclic test was conducted to characterize the BiInSn, and the results show that the material possesses good stability and repeatability. Shaik and Lafdi [32] developed a hybrid heat sink for a spiked heat load. One sink with three different PCM and the other sink with a single PCM is filled, while the PCM is mixed with carbon nanotubes to increase its heat dissipation rate. This PCM chamber is enclosed within the carbon-carbon composite sheets for improved thermal performance. During both constant and pulsed heat loads, sinks with multiple PCM arrangements mixed with nano additives enclosed with carbon sheets yield better results. In addition to the high energy storage rate of the hybrid heat sink, it also dissipated a lot of heat. A composite heat sink filled with carbon nanofillers was analyzed by [33]. They investigated heat sinks with different additive loadings for various pulsed heat loads. Though PCM conductivity is improved by adding carbon fillers, the additive increases the PCM viscosity. Therefore, the natural convection found during melting is weakened. Meanwhile, carbon platelets added to the PCM increase the thermal conductivity and possess less viscosity growth. Hence, nanoplatelets added PCM leads to an improved thermal outcome compared with nanotubes. Under varying heat fluxes, Taghilou and Khavasi [34] presented a PCM-based heat sink. Their study quantitatively observed the effect of natural convection around the heat sink. Along with heat flux from 1000 to 12,000 W/m^2, the heat transfer coefficient also varied in the range of 5–250 W/m^{2}K. An increase in the heat transfer coefficient accelerates the melting rate. Also, the increase in fin number and decrease in fin diameter increases the melting rate, respectively.

In previous research, the authors have examined the impact of enclosure shape on the heat transfer performance of a PCM-filled heat sink. Ye [35] used paraffin as PCM and reviewed the influence of aspect ratio on fluid flow and heat transfer performance. The heating condition was applied at the bottom with a constant temperature of 343.15 K, and the aspect ratios ranging from 0.1 to 10 were considered. As the aspect ratio increases, the melting rate accelerates, and the recirculation during melting is observed clearly. Yang et al. [36] analyzed the significance of the aspect ratio and installation angle of a storage system's efficiency. Aspect ratios ranging from 0.1 to 8 with varying tilted angles of 0^o, 30^o, 60^o, and 90^o are considered. Melting of PCM inside the tank is faster when the heating position is horizontal and slower when the heating position is vertical. When the aspect ratio is greater than 1, a faster melting rate is observed for an inclined heating surface. Similarly, for an aspect ratio lesser than 1, increasing the inclination angle reduces the melting rate. Assessments of aspect ratio on metal foam-embedded PCM heat sinks are done by Behbahan et al. [37]. The square enclosures are not considered to be preferable for the foams inserted PCM chamber, and the optimal aspect ratio raises for higher porosities. 91.66 porosity and 2.11 aspect ratio in a fixed-volume porous enclosure were significantly effective. Choi and Cho [38] investigated the outcome of varying aspect ratios in a rectangular enclosure. At high heat flux, the dominance of the aspect ratio for both liquid and paraffin slurry is more effective. In the paraffin slurry-filled enclosure, efficient cooling was found at an aspect ratio of 0.2 and a mass fraction of 5 %. During melting, the impact of the aspect ratio on a PCM chamber was analyzed by Zhang et al. [39]. The PCM n-paraffin waxes were encapsulated, and the heater plate value was varied from low to high input. In the tank, the conduction is stronger when increasing the height, and temperature variations are observed near the top and bottom walls.

Most of the previous researchers reported pin-finned heat sinks with constant heights. The use of PCM-based heat sinks for steady-state electronic cooling has been explored in previous literature. But, investigations based on different fin arrangements for a pulsating heat load are found less in the literature. This paper compares the impact of modified fin arrangements (i.e., variable height fin heat sinks) over existing fin arrangements (i.e., constant height fin heat sinks) at constant and power surge loads. The power loads are applied along with constant heat load and no-load conditions. Further, power loads are applied at pulsating ON and OFF conditions. The effect of these conditions on a PCM enclosure is discussed using temperature-time history. The thermal performance of both the heat sinks is evaluated and compared based on the experimental results. The geometry of an enclosure becomes crucial for any heat transfer analysis. Later in this study, the aspect ratio of the heat sinks varied numerically. The change in aspect ratio and its influence on both the heat sinks are briefed. By fixing the length of the enclosure, the width, and the height are varied, and the volume remains constant in all cases. Six enclosures ranging from 0.3 to 0.8 aspect ratio for both constant height and variable height fin heat sinks are considered. The outcomes are discussed by the contour images of temperature and liquid fraction of PCM. Finally, in the numerical study, the influence of fin shapes like square, circle, triangle, and diamond is studied. From the numerical results, one can select a better fin configuration heat sink based on the aspect ratio and fin shape.

2. Experimental setup

In Fig. 1, the schematic diagram of the experimental setup is presented. The setup constitutes a computer, DC power supply, data logger, and the finned heat sink. The heat sink is made of aluminum, and the dimensions are 100 mm × 50 mm with a depth of 25 mm. In the heat sink, the PCM cavity is 90 mm × 40 mm with a depth of 20 mm. The heater slot is grooved for 2 mm at the bottom of the heat sink with dimensions of 86 mm × 36 mm.

Based on the previous research [40], an optimal volume fraction of TCE 8 % is chosen. The TCE volume fraction is determined by the ratio of the fin volume to the PCM volume. Two heat sinks consisting of 96 pin fins with constant fin height and variable fin height are shown in Fig. 2. The fins are employed in the heat sink by the milling process. In a constant fin height arrangement, all fins are at the same height of 15 mm. Whereas, for variable fin height assembly, one fin is 20 mm, and the other is 10 mm, and the fins are scattered successively. Both the heat sink comprises fin area dimensions of 2 mm × 2 mm.

The heat sink assembly is covered by cork on all sides except the top side for insulation purposes. On the top surface, an acrylic sheet is placed and fixed over the heat sink assembly by tightening the screw. A rubber gasket is placed between the acrylic and aluminum surfaces to prevent leaks. Thermocouples are placed in the heat sink to measure the heater, wall, and PCM temperatures. A nichrome wire heater wounded over mica sheets generates the power supply to the enclosure. The dimension of the plate heater is 86 mm × 36 mm with a 2 mm thickness, and it is fit into the grove slot at the bottom of the enclosure. A thermal conducting paste with a conductivity of 1.42 W/mK is applied at the slot to increase the conduction pathway. The PCM incorporated in this study is n-eicosane. The DSC analysis was carried out to determine the latent heat capacity of the material. The sample was alternatively heated and cooled in the range of 0–100 °C by a fixed heating/cooling rate of 10 K/min. The procedure is repeated thrice, and latent heat is determined. The properties of all the materials are listed in Table. 1.

All the thermocouples are inserted into the heat sink using Araldite epoxy. Two thermocouples, T_1 and T_2, are located at the base where the heater is attached to the slot. Within the PCM, six thermocouples (T_5, T_6, T_7, T_8, T_9, and T_{10}) are inserted from all sides. Among these six, two thermocouples T_5 and T_6 are at 20 mm height from the base, and another two thermocouples T_7, T_8 are at 10 mm height on the long side of the wall. The remaining two thermocouples, T_9 and T_{10}, are placed from the short sides with a height of 15 mm. All the thermocouples within the PCM are at a distance of 10 mm from each side. Two thermocouples, T_3 and T_4, are located on the long side of the walls to measure the wall temperature. Finally, the last thermocouple is kept outside to measure ambient temperature. The thermocouples are then connected to the data logger, and the positioning of the thermocouples is shown in Fig. 3.

The surge test was conducted manually, and a five-second clearance was provided before and after the power surge load was applied. Next, to calibrate thermocouples, a standard thermometer with a resolution of 0.1 °C is used to measure the accuracy of the thermocouples. In a calibration bath with temperatures ranging from 30 to 70 °C, the error in temperature is within the range of ±0.25 °C. The uncertainty analysis of voltage and current from power input is based on the propagation method of error as mentioned in Eq. (1). The uncertainties in the input heat are measured based on the least count of current ±0.01 A and voltage ±0.1 V. For a 10 W power supply, the uncertainty calculated is ±0.667.

$$\omega_P = \pm\sqrt{\left(\frac{\partial P}{\partial V}\omega_v\right)^2 + \left(\frac{\partial P}{\partial I}\omega_I\right)^2} \quad (1)$$

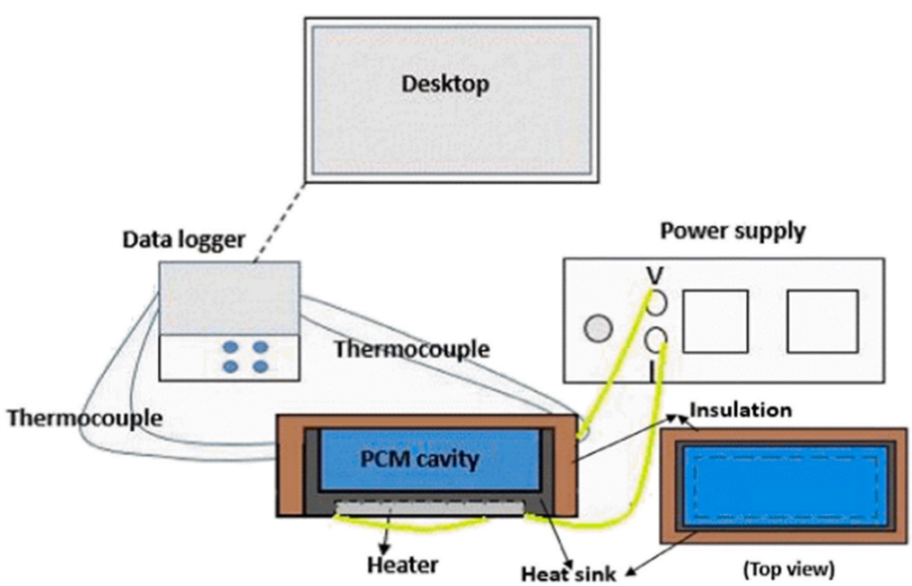

Fig. 1. Schematic of the experimental setup.

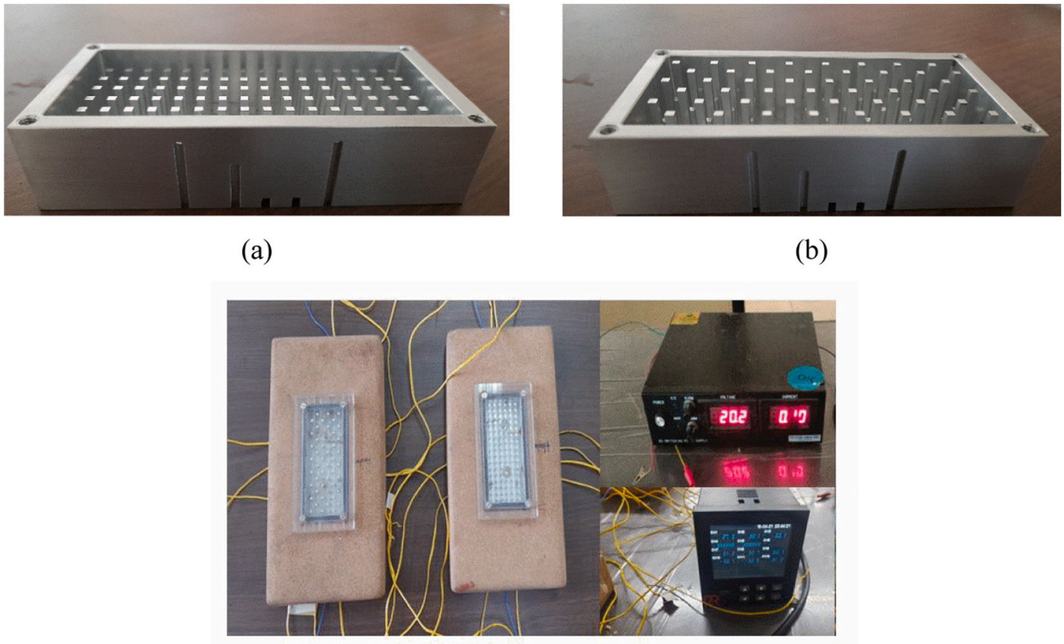

Fig. 2. Photographic display of (a) Constant finned heat sink, (b) Variable finned heat sink, and (c) Heat sink assembly with setup.

Table 1
Properties of the materials [41].

Materials	n-Eicosane	Aluminum	Cork
Specific heat (kJ/kgK)	2200	870	2.05
Thermal conductivity (W/mK)	0.16	200.4	0.05
Melting point (°C)	36.5	660	–
Density (kg/m^3)	780	–	–
Viscosity (kg/ms)	0.00355	–	–
Coefficient of thermal expansion (1/K)	0.001	–	–
Latent heat (J/kg)	247,000	–	–

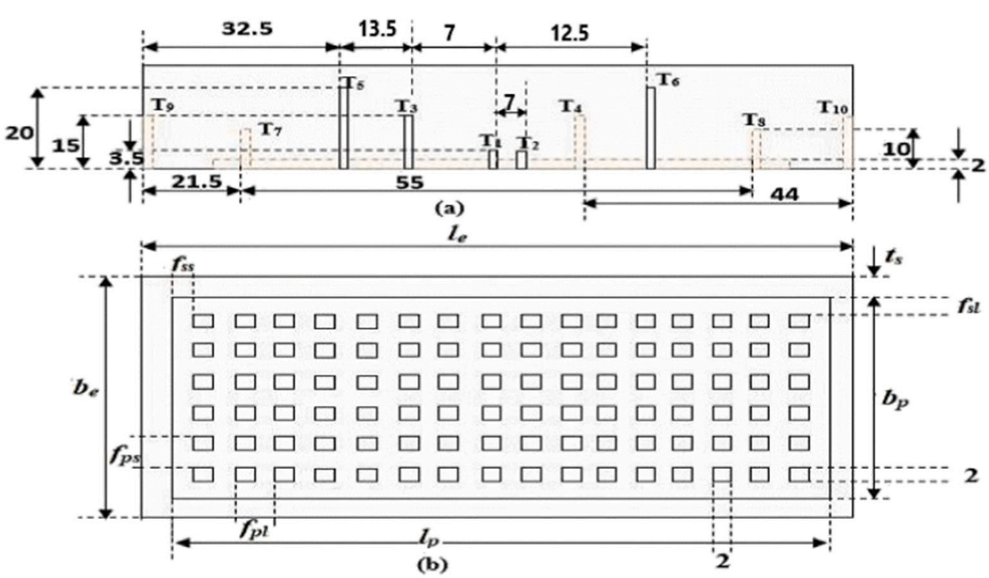

Fig. 3. Thermocouple positioning for both the heat sinks with dimensions in mm (a) front view and (b) top view.

3. Numerical formulation

During melting/solidification, PCM phase change simulations are based on enthalpy-porosity theory. Based on this technique, the governing equations are solved. In the numerical study, the thermal properties, such as thermal conductivity, specific heat, and viscosity, are kept constant. The Boussinesq approximation accounts for the density variation due to natural convection. The approximations included in this study are flow laminar, inviscid, and transient. The volume expansion/shrinkage of PCM during a phase change is neglected in the analysis. The governing equations are [42],

Continuity and Momentum equations:

$$\frac{\partial \rho_p}{\partial t}+\frac{\partial(\rho_p u)}{\partial x}+\frac{\partial(\rho_p v)}{\partial y}+\frac{\partial(\rho_p w)}{\partial z}=0 \tag{2}$$

$$\rho_p\frac{D\vec{v}}{Dt}=\mu\,\nabla^2\vec{v}-\nabla \mathrm{P}^*+\rho_p\beta_0(T_m-T)\,\vec{g}+A\,\frac{(1-\Phi)^2}{(\Phi^3+\lambda)}\vec{v} \tag{3}$$

Energy equation:

$$\frac{\partial}{\partial t}(\rho H)+\nabla\bullet(\rho\,\vec{v}H)=\nabla\bullet(k\nabla T) \tag{4}$$

$$\Phi=0, if\ T<T_s \tag{5}$$

$$\Phi=1, if\ T>T_l \tag{6}$$

$$\Phi=\frac{T-T_s}{T_l-T_s}\ if\ T_s<T<T_l \tag{7}$$

The last term in Eq. (3) is the source term, which controls the velocity damping during solidification. A is the mushy zone constant, and λ is the computational constant to prevent dividing by the number zero in the denominator. Their corresponding values are 10^5 and 0.001, respectively. At the computational cell, the symbol Φ is the liquid fraction which provides the volume ratio of liquid PCM to the total PCM. The enthalpy H in Eq. (8) includes both the sensible and latent enthalpies of the material. T_r and h_{ref} are the reference values of temperature and enthalpy, respectively.

$$H=h_s+\Phi L_p \tag{8}$$

$$h_s=h_{ref}+\int_{T_r}^{T}c_p\mathrm{d}T \tag{9}$$

The conservation equations of the PCM are solved by the commercial software ANSYS Fluent 19, which works based on the finite volume method. The pressure and velocity equations are coupled by the SIMPLE scheme and are employed in this simulation. The second-order upwind scheme solves the discretization of momentum and energy equations. The convergence criteria for continuity, momentum, and energy equations are 10^{-5}, 10^{-5}, and 10^{-8}, respectively.

During the charging cycle, the initial state of PCM is solid. At $t=0$, $T=T_{HS}=T_{PCM}=300$ K. The boundary condition at the top surface, z = 0.025, $\frac{\partial T}{\partial z}=\frac{\partial T_{HS}}{\partial z}=\frac{\partial T_{PCM}}{\partial z}=0$. The remaining walls, excluding the heater slot surface, has $\frac{\partial T_{HS}}{\partial z}=0$. At the surface contact with the heater, a constant wall heat flux condition $-k_{HS}\frac{\partial T_{HS}}{\partial z}=\dot{q}=1292\ \mathrm{W/m^2}$ is applied.

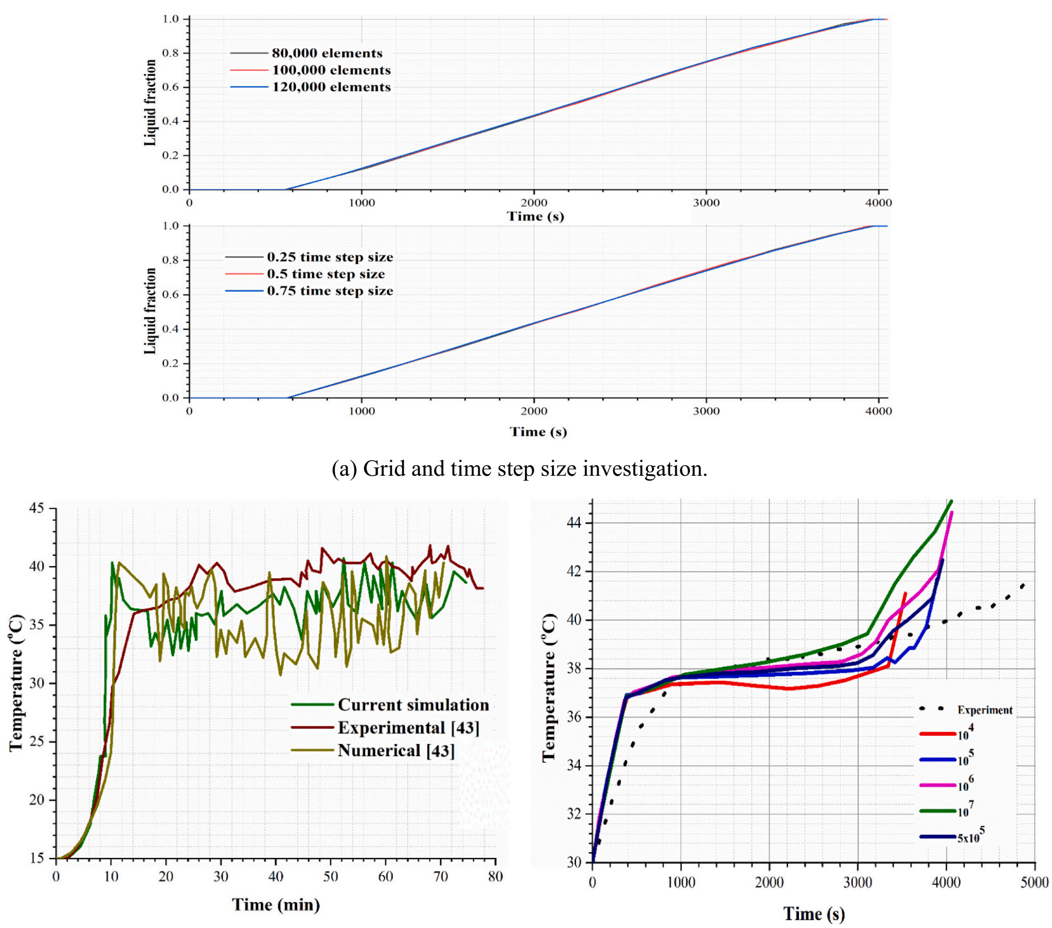

(a) Grid and time step size investigation.

(b) Validation

(c) Numerical and experimental comparison

Fig. 4. Computational analysis.

Similarly, during discharging cycles, the PCM is in a liquid state. At t = 0, $T = T_{HS} = T_{PCM} = 323$ K. A constant wall temperature condition of 300 K is applied at the heater slot surface. The remaining wall surfaces are at adiabatic conditions similar to charging cycles.

4. Grid independence study and validation

4.1. Grid independence study

The numerical accuracy for a transient simulation is evaluated by selecting different grid sizes and time-step sizes. The grid sizes of 80,000, 100,000, and 120,000 elements are selected for the grid independence study under a time step size of 0.5 s. Subsequently, the time step sizes are varied by 0.25 s, 0.5 s, and 0.75 s with 100,000 elements. These selected sizes are employed in the constant height fin heat sink, and the results are plotted. The liquid fraction of PCM is plotted against time intervals in Fig. 4 (a). The trend is very similar, and the deviations are negligible for both cases. Hence, an element size of 100,000 and a time step size of 0.5 s are selected in this study.

4.2. Numerical validation

The numerical model developed is investigated by comparing the results with the work of Parsazadeh and Duan [43]. In their investigation, both the experimental and numerical works were carried out for the charging cycle using coconut oil as PCM. Inside a 60 × 60 mm enclosure, initially, the PCM is at a solid state with a temperature of 15 °C. A constant wall temperature condition with 55 °C is applied at the bottom of the enclosure. The temperature within the PCM at a location of 5 mm from the left side of the enclosure and at a height of 10 mm is noted down. Similar geometry with the same initial and boundary conditions and PCM temperature locations are considered for validation purposes. In Fig. 4 (b), the PCM temperature at various time intervals is plotted. A maximum deviation of 6 % was observed between the experiment and the current simulation. In both numerical cases, the initialization of melting occurs earlier compared to the experiment. This is because the properties employed in the numerical study do not vary with temperature and remain constant throughout the cycle. Whereas in experiments, the properties vary with increasing temperature.

4.3. Present experimental vs. numerical comparison

The mushy zone constant captures the flow within the sink, and the morphology of the mushy zone is defined by this constant. However, the value of A varies for different materials when using the enthalpy porosity method. Here, in this study, the mushy zone constant values considered are 10^4, 10^5, 5×10^5, 10^6, and 10^7. Also, the experimental result is compared with the varying mushy zone constant values for a constant fin height heat sink. The initial and boundary conditions taken for experimental analysis are accounted for in the numerical study. A power input of 4 W is applied, and the variation in the base temperature of a heat sink is presented in Fig. 4 (c). From the figure, it is clearly seen that the value of 'A' influences the melting of PCM. This is due to the effect of the mushy zone constant at the liquid PCM region and the mobility disturbance of PCM during phase change. As the value of A increases from 10^4 to 10^7, the temperature curve increases during the latent heat period. Whereas the completion of the latent heat period is also altered by varying the constant value. The longer latent heat and the steady temperature during the latent heat period are observed when the value is 10^5. Next, comparing the values with experimental results, the base temperature obtained by numerical simulation is faster than the experimental run because of the unavoidable heat dissipation towards the environment in experiments. Whereas in numerical simulation, there is no heat loss to the surroundings. This depicts the delay in initialization and completion of melting during the experimentation. But, the latent heat period of 10^5 constant value and the experimental case is almost equal other than the differences in the initialization of melting. Additionally, the constant properties assumptions for the material specified also have a slighter impact on the temperature distribution. From these understandings, the value of A considered in the numerical study is 10^5.

5. Results and discussion

5.1. Experimental results

5.1.1. Constant heat load

The heat flux is varied from 4 W to 50 W, where 4 W–10 W is considered a light load and 20 W- 50 W is considered a power load. The ambient temperature for all the experiments is close to 26 °C. The heat sink base temperature of both enclosures is compared in Fig. 5. The heat sink base temperatures are calculated based on the average of two thermocouples placed at the bottom of the sink surface near the heater. For all heat fluxes, the completion of melting is faster in the variable height fin heat sink. This faster melting is due to the significant effect of fin height non-uniformity in the enclosure, which accelerates the charging cycle. In variable height fin heat sink, since half of the fin heights are near the top surface, it increases the heat transfer within the PCM at the top side. In a constant height fin heat sink, the fins are the same size, and the top side PCM in the enclosure takes longer to melt. In the absence of fin exposure at the top side, PCM melts based on its own thermal conductivity, which is generally less. Hence, the heat transfer from the heater to the PCM is reduced; thus, a longer melting time is observed.

When the heat load increases, the initiation time of the phase transition reduces. This is due to the high heat generation to the enclosure, which melts the PCM at a faster rate by overcoming its poor thermal

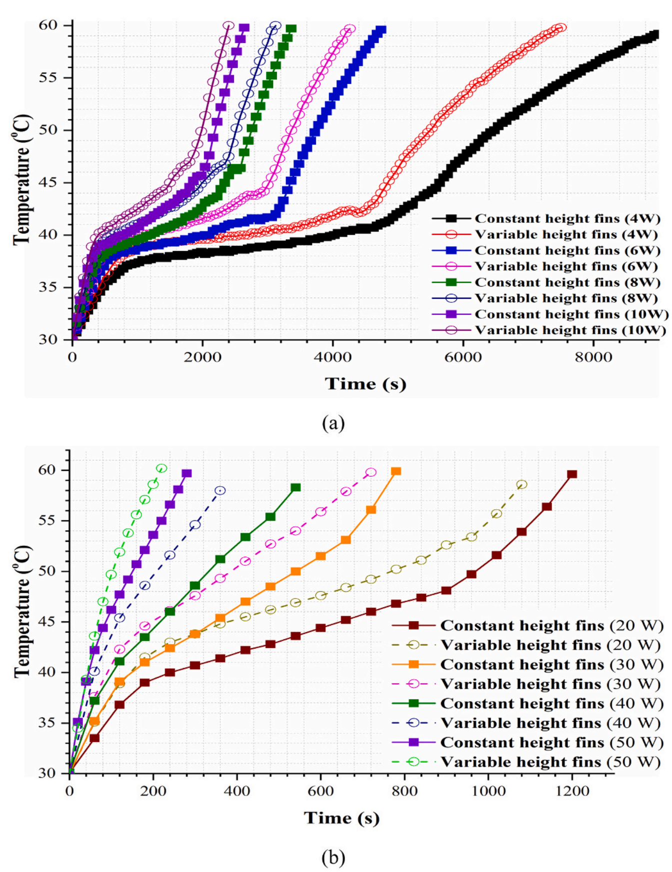

Fig. 5. Heat sink base temperature against time intervals for various heat inputs.

conductivity. This result is seen for both the heat sinks, but for variable height fin heat sinks, it is higher compared with constant height fin heat sinks. The reason is in the variable height fin heat sink, the thermal conductance offered by the fins to the PCM is more and initiates the phase transition at an earlier stage. The thermal conductance of the fins in the heat sink refers to how effectively the heat is transferred from the sink to the phase change material (PCM) and promotes faster phase transition (melting) in the PCM. The fin volume in both the heat sinks are same, but the heat surface area exposed to the PCM is more for the variable fin height heat sinks. This area covers the top surface of the sink, which is not covered by the constant fins, and provides better overall melting of PCM. At the same time, the temperature plots at power loads show a faster melting rate. In the loads (30 W- 50 W), it is observed that the latent heat period of PCM vanishes in both heat sinks. Because the heat supplied to the PCM is high enough to overcome the latent heat of fusion, only sensible heating is observed. Hence, the phase transition happens rapidly at high power loads compared with low power loads. For any loads in Fig. 4, the trend follows the same for both

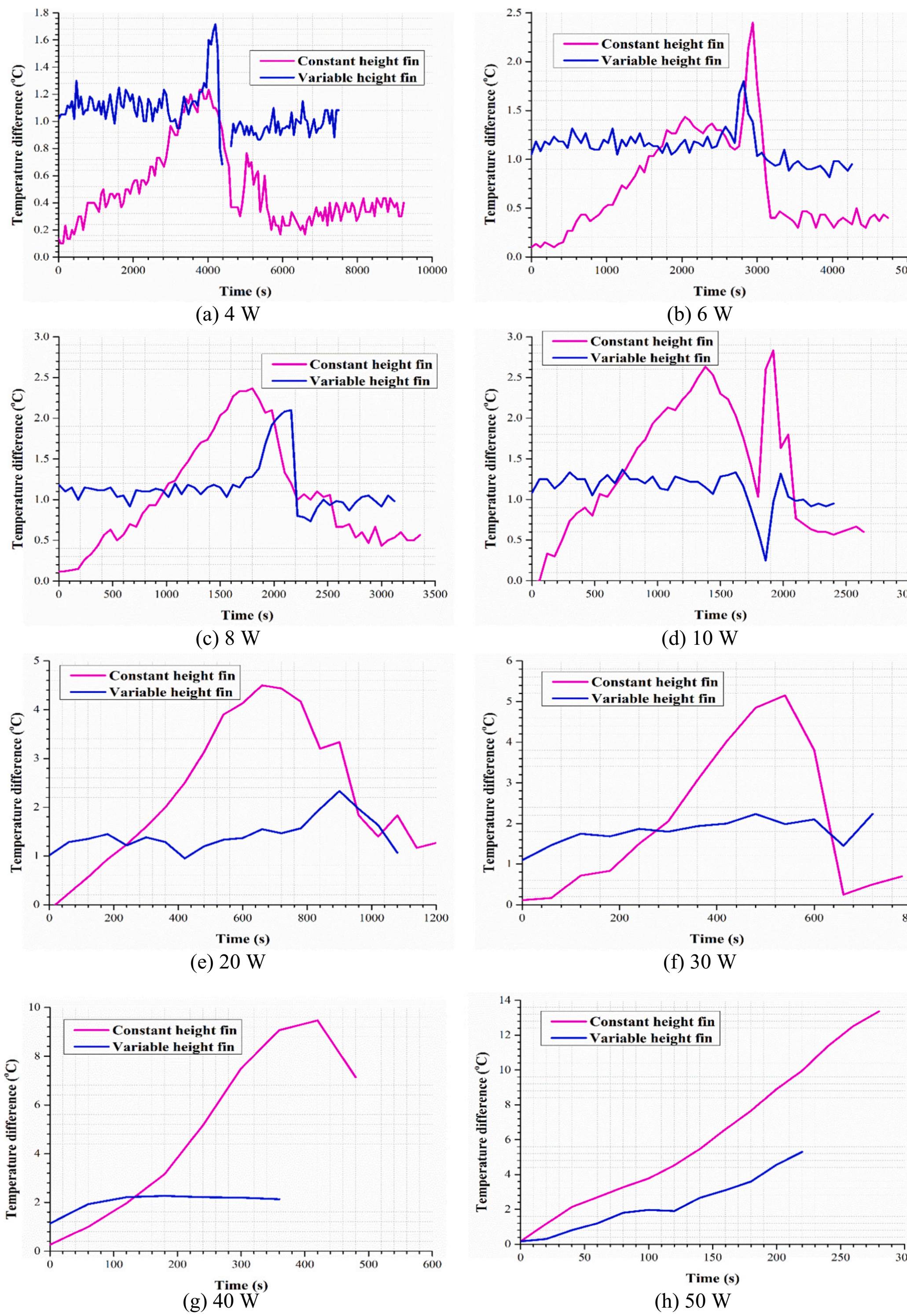

Fig. 6. Temperature difference between the PCM and side wall temperature at various heat inputs.

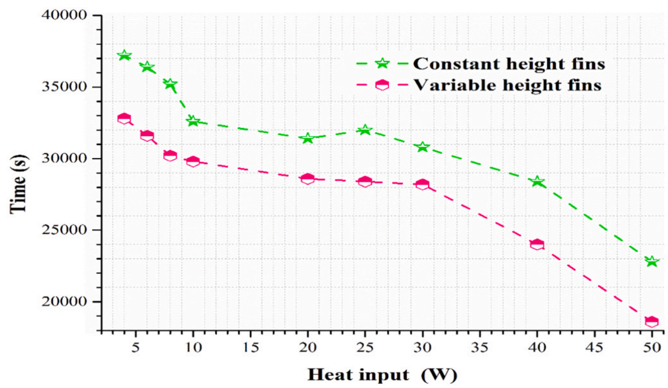

Fig. 7. Solidification time to reach 30 °C for different heat inputs.

the heat sinks.

A figure is plotted to understand the heat transfer within the PCM and the heat transfer through the side walls. In Fig. 6, the temperature difference between the PCM and sidewall temperature of the heat sink until the heat sink base reaches 60 °C is reported. The average temperature of six thermocouples (T_5, T_6, T_7, T_8, T_9, and T_{10}) kept in PCM and the average of two thermocouples (T_9, T_{10}) placed on the walls are considered here. In these cases, the variable fin height has a higher temperature difference at the initial stage. But, the deviation after the initiation of melting is found to be less. This shows the uniformity of heat distribution within the enclosure. This is due to the fin exposed area within the enclosure being high; at all heights, there is a uniformity of heat transfer. Whereas in the constant height fin heat sinks, the initial difference is less, but once the melting starts, the temperature rises with time. There is no uniform temperature distribution in the heat sink between the side walls and the PCM compared to variable height fin heat sinks. The peak temperature difference is obtained for both cases, which implies the latent heat zone, and once the post-sensible heat zone starts, the temperature falls and attains a lesser difference.

Then both the heat sinks are evaluated during the discharging cycle at various heat fluxes. In Fig. 7. the time taken for the heat sink base to reach 30 °C for both the heat sinks is plotted. Unlike melting, the solidification of PCM takes a longer time because of its poor thermal conductivity and no natural convection to enhance the solidification. Variable height fins show a faster discharging rate than constant height fins. The reason is similar to melting; the heat transfer region of PCM with fins was found to be high for a variable height heat sink. As the heat flux increases, the time taken for the PCM to get solidified is reduced. This is because, at higher heat flux, the heat sink base temperature expands suddenly and achieves 60 °C sooner. When the heater is then

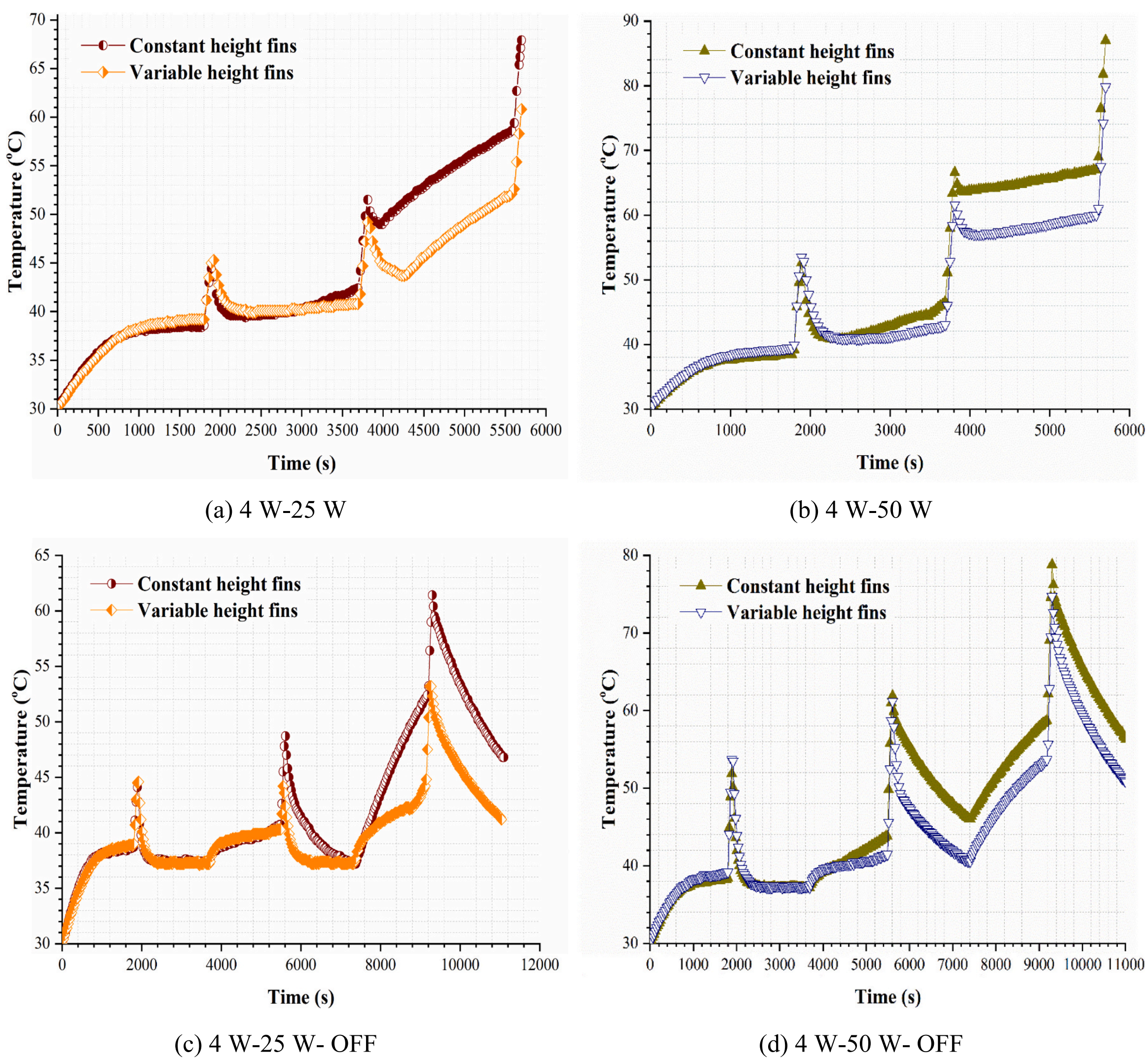

Fig. 8. Heat sink base temperature v/s time for a combination of 4 W- power load (a) 25 W (b) 50 W and combination of 4 W- power load - 1800 s OFF condition for (c) 25 W (d) 50 W.

switched off, the heat is transferred to the PCM and side walls, and it attains 30 °C faster than other walls and PCM. But at low heat flux, the heat sink base temperature, along with the side wall and PCM temperature, reaches 30 °C simultaneously with smaller gaps.

5.1.2. Power surge with constant load

A constant load of 4 W for 1800 s, then continued by power load for 100 s, is applied. Next, a constant load of 4 W for 1800 s, continued by a power load for 100 s, and the solidification time of 1800 s are recorded, unlike the previous one. Both the durations considered for this study are taken from the previous literature [32,44] as a reference to obtain the performance of two heat sinks. The power surge of 25 W and 50 W are considered, and three cycles were run under similar conditions. In Fig. 8 (a) and (b), without solidification time, the base temperature of constant height fin and variable height fin heat sinks are compared. The variable height fin heat sink attained the peak temperature in the first cycle. The

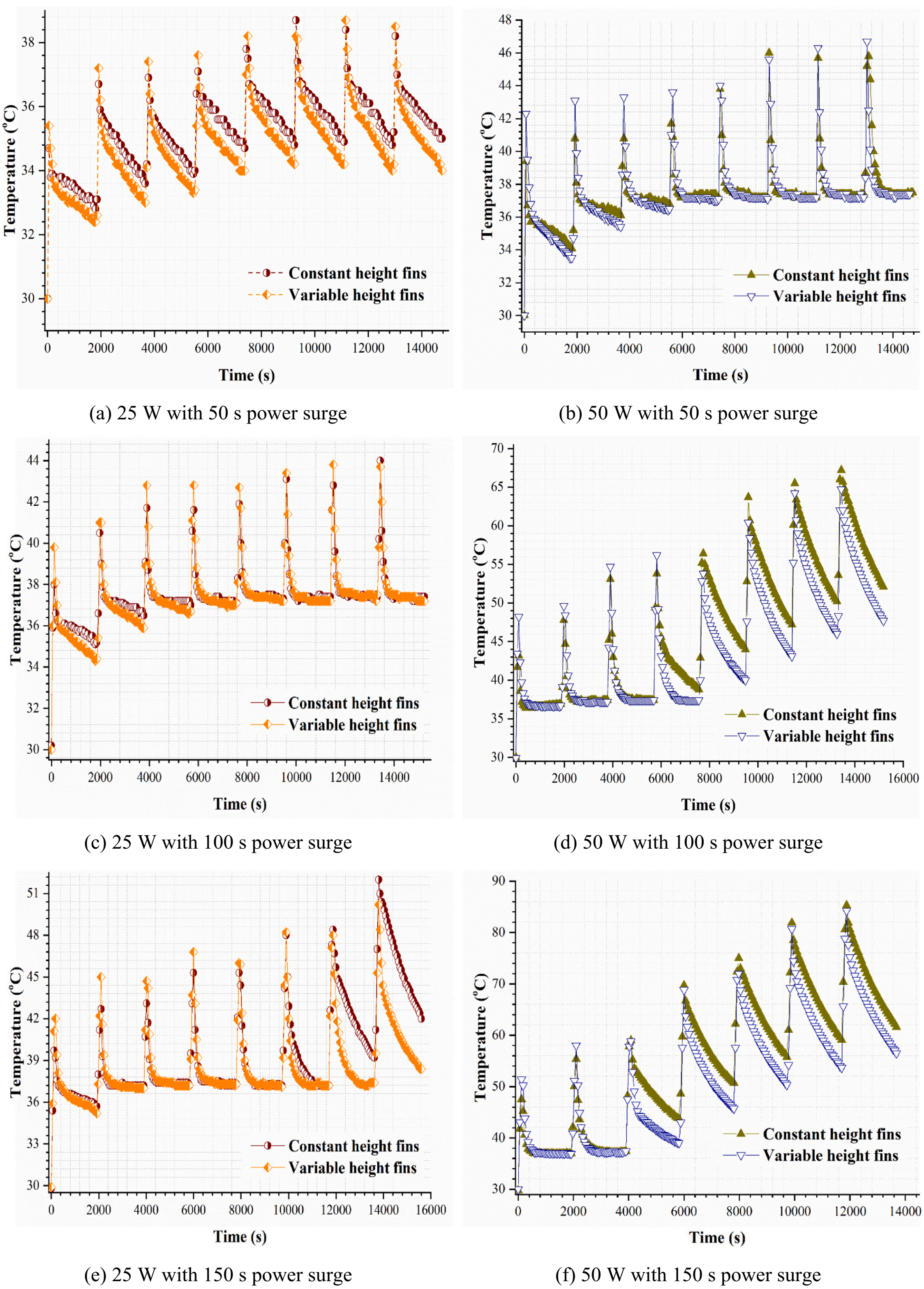

(a) 25 W with 50 s power surge

(b) 50 W with 50 s power surge

(c) 25 W with 100 s power surge

(d) 50 W with 100 s power surge

(e) 25 W with 150 s power surge

(f) 50 W with 150 s power surge

Fig. 9. Power surge with different durations of 50 s, 100 s, and 150 s at 25 W and 50 W inputs for Heat sink base temperature against time.

reason is due to the faster melting occurring in a variable height heat sink with the help of non-uniform fin heights. Once the power surge is removed and constant load is applied, the PCM comes to the latent heat period, where it is not completely into the liquid state. Hence, the PCM is at a lower temperature when the second cycle power load starts for both the heat sinks. But comparatively, the PCM temperature for the variable height heat sink is lower at the end of the second cycle (constant load of 4 W) due to its higher absorption rate. This helps the variable height fins at the second pulsed load to obtain a lower peak temperature than constant fins. This high heat transfer within the variable height fin heat sink is continued with increasing cycles. Also, the differences in the peak temperature of the two heat sinks are increased further. This is observed in the third cycle, where the peak temperature of the constant height fin is 68 °C, and the variable height fin is 61 °C at 25 W. At 50 W, the peak temperatures are 87 °C and 80 °C for constant and variable height fins, respectively.

In the next cycle, the constant load and the power load are added along with the solidification time of the 1800 s. The heat sink base temperature of both the heat sinks is plotted in Fig. 8 (c) and (d). The first cycle is similar to the previous one, where the variable height fin with a higher melting rate melts quicker and attains a higher peak temperature at constant and power loads. But, during the resting time, the PCM solidifies and almost reaches the temperature of 36 °C. Hence, at the beginning of the second cycle, the PCM is in a solid state, but the temperature is higher than the initial temperature. Due to the higher solidification rate of the variable height fin heat sink, the initial temperature is lower than the constant fin heat sink when the second cycle starts. Consequently, the peak temperature value is also shifted towards a constant fin heat sink. Then the cycle is continued and is noted with a higher temperature difference between the variable and constant height fins. The peak temperature differences observed between constant and variable height fins at 25 W and 50 W at the end of cycles are 9 °C and 6 °C, respectively. At these varying loads of constant and power loads, variable height heat sinks perform better than the constant height fin heat sinks. The explanation behind this better performance is that the fins placed at different heights within the enclosure reduce the resistance offered by the PCM at all heights and enhance the melting/solidification process.

5.1.3. *Power surge- ON and OFF condition*

Next, only power loads with varying durations and resting times are applied, neglecting the constant load. The power load is employed for a duration of 50 s, 100 s, and 150 s, and the OFF condition is 1800 s for all time durations. In Fig. 9, the heat sink base temperature of both heat sinks at 25 W and 50 W power loads are represented. During the 50 s power surge, for almost all cycles, the peak and the least temperature are observed for variable height fins. The variable height fin heat sink melts the PCM during load time and solidifies the PCM during a resting time faster than constant height fins by increasing its thermal conductance within the PCM and heat transfer between the walls and the PCM. At a power load of 50 W, with a 50 s duration, the peak temperature is observed for variable height fins except for the 6th cycle, and the least temperature is found for variable height heat sink at all cycles. At the beginning of the cycles, the peak temperature difference between the heat sinks is high, and after the 5th cycle, it becomes lesser. This is because the constant height fins show slower melting, reducing its time to attain peak temperature for a certain cycle. Also, it tries to compensate for the slower solidification rate up to certain cycles. This compensation can be seen for 100 s and 150 s at the 5th cycle and 4th cycle in Fig. 8 (d) and (f), respectively. Once it crosses that cycle, the peak temperature is shifted towards the constant height fins. But, this shift is not observed for 50 s durations because of less duration, but the temperature difference between them is reduced a lot. Similarly, for 25 W power loads, the peak temperature shift occurrence can be seen at 150 s at the 7th cycle. During the 100 s duration at the 8th cycle, the constant height fin reaches peak temperature than variable height fins with a slighter margin. But at 50 s, the peak temperature shifts to constant height fins appear at the 6th cycle, and then again, the peak temperature is shifted to variable height fins. The reason is the same as the 50 W power load, where the time duration is not enough for variable height fins to overcome the slow solidification rate of constant fins. So, from this explanation, with the increasing power surge and time duration of these surges, constant cycles show a higher peak temperature after a few cycles than variable height fins.

The experimentation was conducted on the existing constant height fin heat sinks and proposed variable height fin heat sinks. The volume of PCM and the fin volume remains constant, and only the fin height is varied in the enclosure. First, at constant heat load with different heat fluxes, the results are obtained based on the temperature-time graphs. Next, power surge load is applied under different scenarios, and using plots, the results are discussed. From the analysis, it is understood that considering all types of heat load at different conditions, variable height fin heat sink performs better than conventional constant height fin heat sinks. By considering these outcomes, then a numerical study is carried out to study the effect of enclosure aspect ratio and fin shapes on both the heat sinks. The cost of making different enclosures and changing the fin shape is not economical and time-consuming. Hence in this paper, the impact of enclosure aspect ratio and fin shapes are interpreted numerically.

5.2. *Numerical results*

5.2.1. *Aspect ratio effects*

The aspect ratio of the PCM-based enclosure is discussed here under numerical study. All applications have different configurations, and the heat sink dimensions will be varied accordingly. Hence, the influence of aspect ratio on a heat sink is crucial. The impact of fin arrangement on a PCM-based heat sink is explored by varying the aspect ratio. The comparison of variable and constant height fin heat sinks is evaluated for different aspect ratios. The detailed dimensions of the aspect ratio considered in this study are tabulated in Table 2. A constant load of 4 W for all aspect ratio enclosures is applied at the bottom, and other sides

Table 2
The enclosure dimensions in mm for different aspect ratio.

Aspect ratio	h_f	l_e	b_e	h_e	l_p	b_p	f_{pl}	f_{ps}	f_{sl}	f_{ss}	n_f
0.3	constant = 30 variable = 40,20	100	30	45	90	20	3.5	4	3	2.5	48
0.4	constant = 20 variable = 25,15	100	40	31.67	90	30	7	4.5	2.75	5.5	72
0.5	constant = 15 variable = 20,10	100	50	25	90	40	5.5	6	4	2.75	96
0.6	constant = 12 variable = 16,8	100	60	21	90	50	6	6	3	2	120
0.7	constant = 10 variable = 13,7	100	70	18.3	90	60	5.5	6.5	3	2.75	144
0.8	constant = 8.565 variable = 10.565,6.565	100	80	16.42	90	70	6	5.5	3.75	5	168

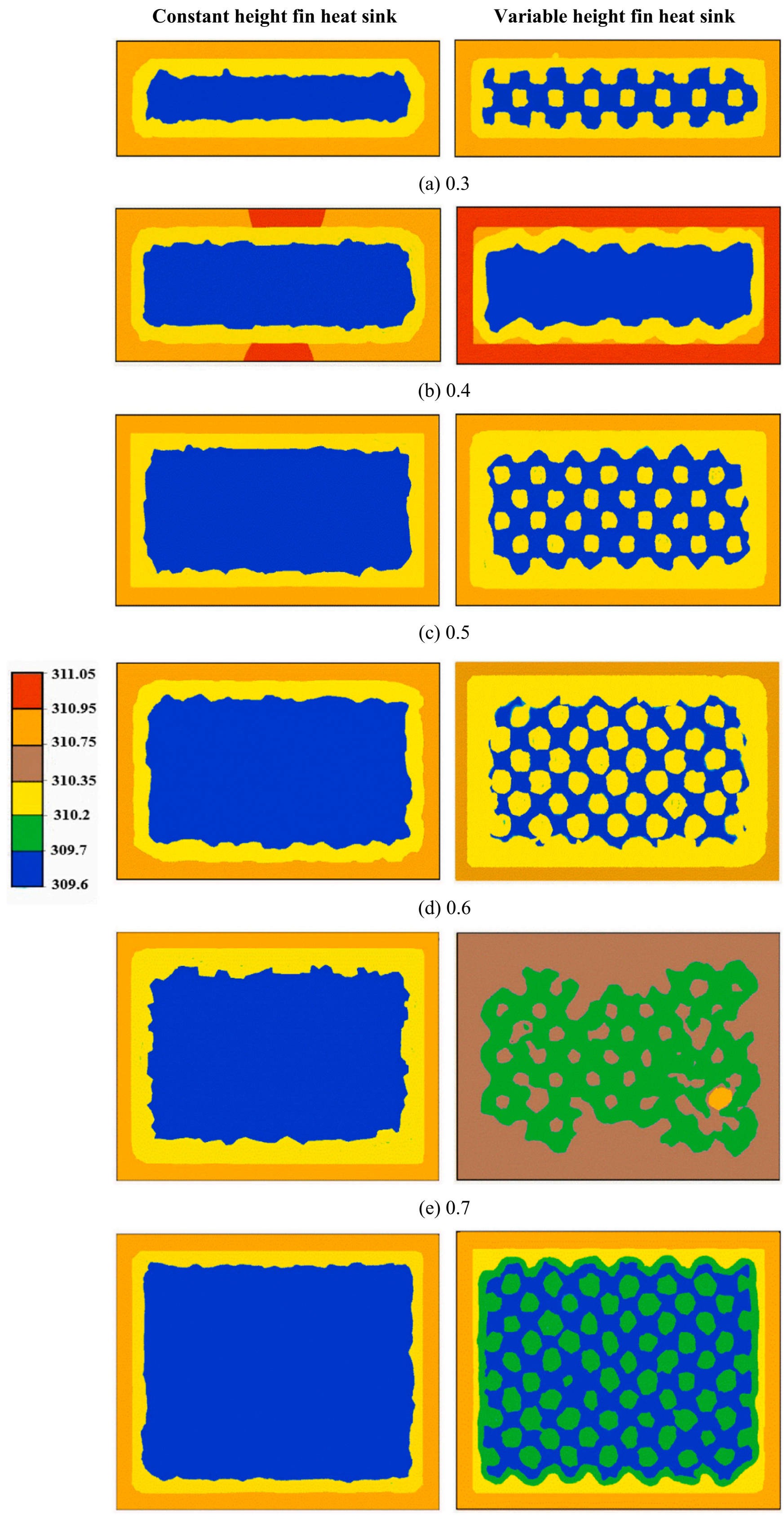

Fig. 10. Temperature contours at 3000 s for both heat sinks with various aspect ratios.

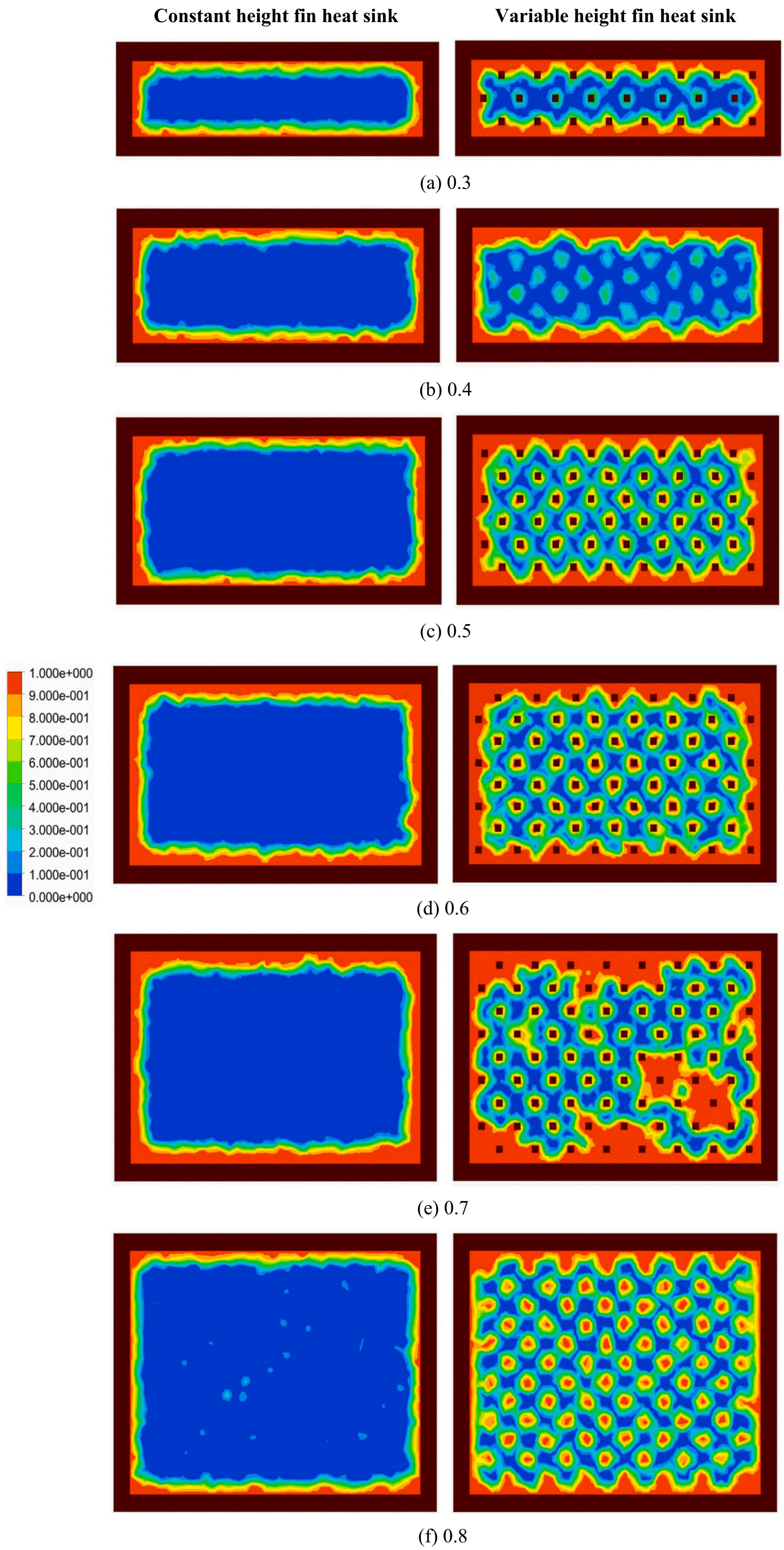

Fig. 11. Liquid fraction contours at 3000 s for both heat sinks with various aspect ratios.

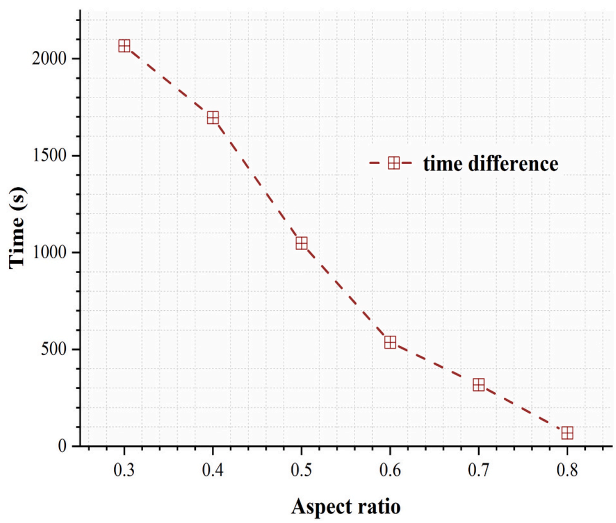

Fig. 12. Time difference between the heat sinks for the completion of a discharging cycle.

are left to adiabatic condition. Initially, the PCM is in a solid state, and the temperature is 300 K during the charging cycle. Instead of plotting graphs, contour images of temperature and a liquid fraction are considered in view of visualization effects. The contour images of temperature and liquid fraction from the top view for all aspect ratios at 3000 s are listed in Figs. 10 and 11.

The constant height fin heat sinks are placed on the left side, and the variable height heat sinks are placed on the right side of the figure. From the temperature contours, for all cases, it is seen that the temperature at walls is almost the same, but the temperature distribution within the PCM is varied. As mentioned in the experiments, the temperature distribution within the PCM in a variable height fin heat sink is more. The reason is due to its higher surface area because of fin distribution throughout the enclosure. Hence in a variable height fin heat sink, the PCM absorbs more heat from the fins and side walls compared with a constant height fin heat sink. Simultaneously, at the same time interval, the liquid fraction is observed. Due to its high-temperature distribution within the PCM, the variable height fin heat sink melts the PCM more quicker. This quicker melting noticed at the top surface increases the overall melting rate of the enclosure. Eventually, the completion of melting is accelerated in the variable height fin heat sink.

Correspondingly, the discharging cycles of these enclosures are also investigated. In the discharging cycle, the PCM is in a liquid state, with a temperature of 323 K. The boundary condition of 300 K is applied at the enclosure bottom, and the other sides are insulated. Fig. 12 shows a time difference between the constant and variable height fin heat sink to complete solidification. From the figure, the aspect ratio increases from 0.3 to 0.8, and the time difference to solidify completely is also reduced. The reason behind this is that when the aspect ratio is less, the height of the enclosure is very high. This leads to a large difference between the fin heights and enclosure heights. The variable height fins with different heights are able to transfer heat at the top position than the constant height fins. For instance, considering a 0.3 aspect ratio, the enclosure height is 45 mm, whereas the constant height fin heat sink has a fin height of 30 mm. But for the variable height fin heights, one fin height is at 40 mm and the other at 20 mm; this increases the heat transfer rate to

Table 3
The dimensions for different fin geometry in mm.

Geometry	Thickness	f_{pl}	f_{ps}	f_{sl}	f_{ss}
Square	t = 2	5.5	6	4	2.75
Circle	d = 2.25	5.25	6.25	3.25	4.5
Diamond	w = 2, h = 4	5.5	6	3	2.75
Triangle	w = 4, h = 2	5.5	6	4	1.75

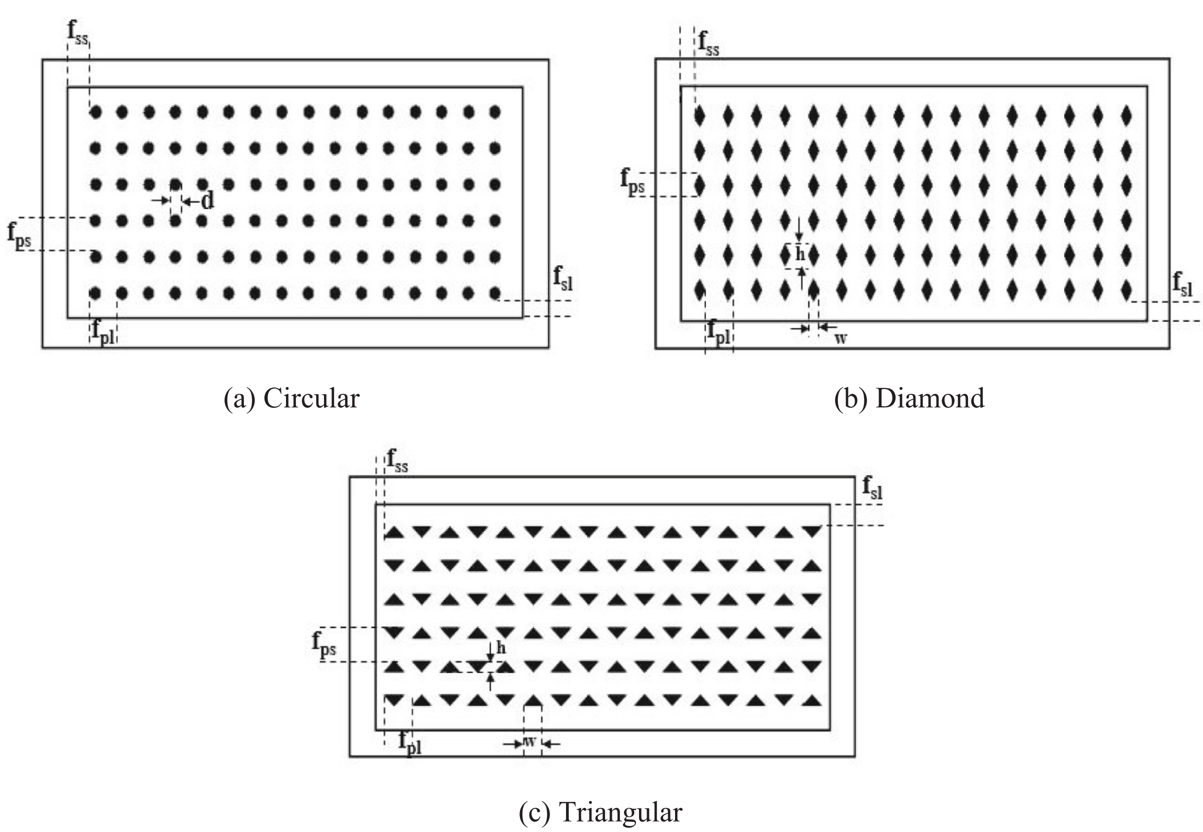

Fig. 13. Sketch of different fin shape.

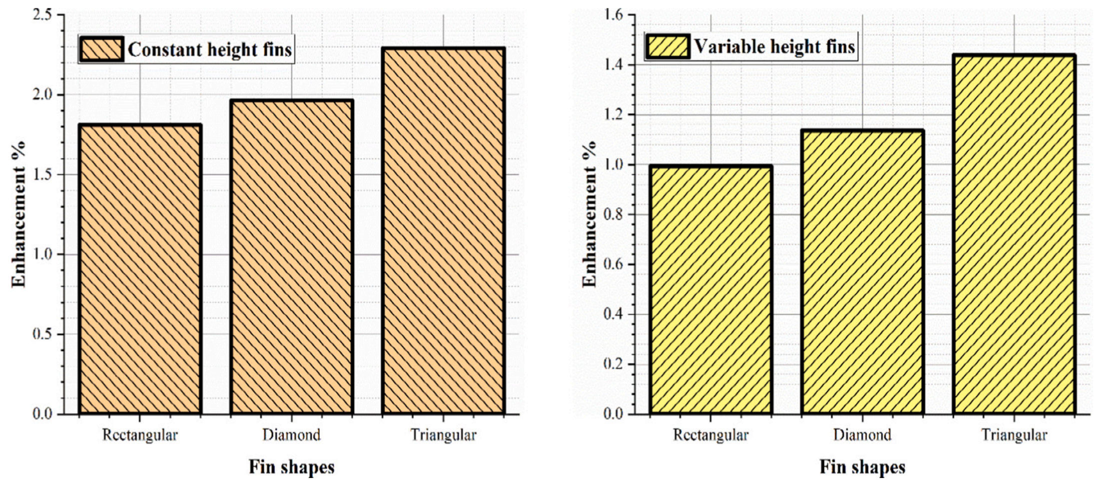

(a) constant fin heat sink (b)variable fin heat sink

Fig. 14. Enhancement percentage during melting for different fin geometry.

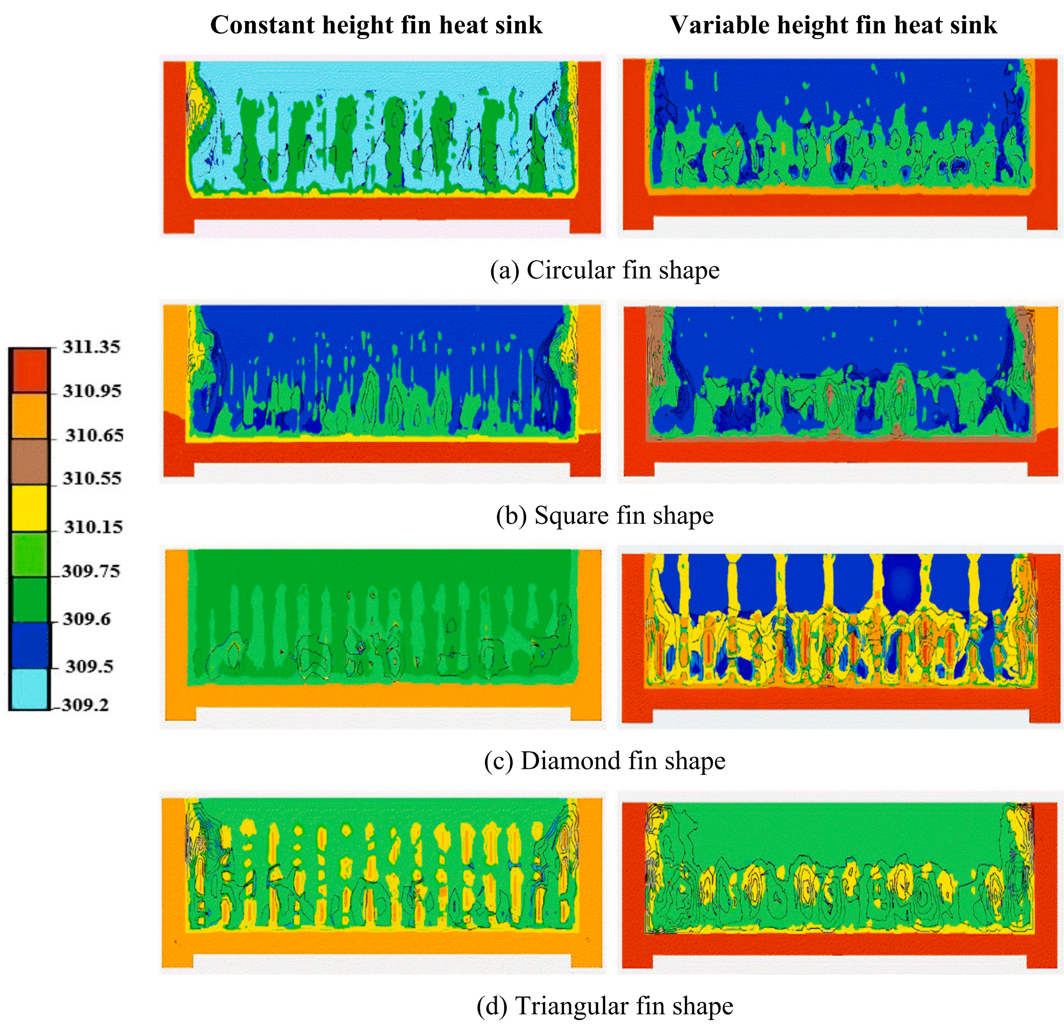

Fig. 15. Temperature and velocity contours for different fin shapes at 3000 s.

a higher range within the enclosure. Hence at a lower aspect ratio, the variable height fins dominate the solidification process. But when the aspect ratio is at 0.8, the time difference is almost 100 s. This is due to the shortened enclosure height; within that enclosure, the fin height does not influence significantly.

5.2.2. *Fin shape effects*

Following the investigation of the aspect ratio, the effect of fin shapes is also assessed. The various fin configurations involved in this study are square, circular, diamond, and triangular. The sketch of different fin shapes is shown in Fig. 13, other than the rectangular shape, which is

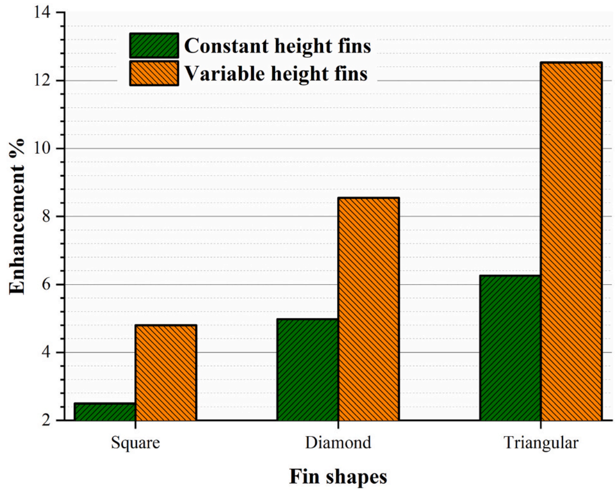

Fig. 16. Solidification enhancement percentage for different fin shapes.

already presented in Fig. 3. The enclosure of both constant and variable height fin heat sink with an aspect ratio of 0.5 is considered.

The fin volume for all shapes is kept constant, and the shape geometries are incorporated into the Table. 3. During the charging process, with the heat load of 4 W, the heater temperature to attain 50 °C against time is noted. In Fig. 14, the enhancement percentage between the shapes is plotted with a circular fin heat sink as a reference. The circular fins have no sharp edges, and their blunt surface has less influence on the melting process. Therefore, the circular fin heat sink shows a longer melting and a longer time for the base to reach the prescribed temperature. Hence among all the shapes, circular fins are used as a reference.

The enhancement percentage of fins to reach 50 °C is defined as the percentage of the time difference between the circular fin and other fin shapes to the circular fin time. A significant deviation was found among other shapes to the circular fin in both heat sink cases. Among the shapes, the triangular fin reaches the 50 °C temperature quicker. Triangular fins have a higher enhancement rate of 2.29 % for constant fin heat sinks and 1.43 % for variable heat sinks. The reason is the arrangement of triangular fins, i.e., in the successive spots, fins are inversely distributed and occupy a higher surface area. This increase in surface area results in a higher heat transfer rate compared with other shapes. Overall, the time difference is very less among these three fins, and the enhancement percentage is found to be less during melting. The time obtained for both the heat sinks to reach 50 °C is different. In constant height fin enclosure, the enhancement percentage is higher compared to the variable height fins. The reason is that in variable height fin heat sink, the fins are distributed throughout the height of the enclosure, and conduction dominates. This results in less convection at the top, though the fin shape is modified, and fewer gaps in temperature are obtained. But in constant height fins near the top surface, the fins are not found, and natural convection has a stronger influence than conduction. The contours of temperature and velocity for different configurations are illustrated in Fig. 15. A mid-section plane at the longer side was considered to examine the effects. At 3000 s time intervals, these figures are plotted where the differences are distinguished. The figure shows that the triangular fin possesses uniform temperature distribution and more liquid motion for both heat sinks. The reason is that the contact area with the PCM is more for triangular fin shapes. In variable height fin heat sinks, more liquid motion is observed for all cases because the melt portion of PCM is higher for this case.

During the discharging process, the effect of fin shapes is evaluated. The aforementioned boundary condition in aspect ratio investigation during solidification is applicable here. Fig. 16 shows the enhancement percentage of both heat sink cases for the solidification process. Here, the enhancement percentage is the time taken to completely solidify the respective fin shapes difference from the circular fin shape time to the time taken by circular fins. Here, similar to the charging process, the circular fin is kept as a reference due to its slow discharging rate. Unlike melting, a significant effect of modified fin shapes is observed in solidification. Among all the fin shapes, for both heat sink cases, triangular possess a higher enhancement of 6.25 % for constant fins and 12.5 % for variable fins. This is due to the higher surface area exposed within the PCM for triangular fins. This higher exposure leads to high conduction and accelerates the solidification rate. When comparing both the heat sinks, variable height fins show higher enhancement due to their fin arrangement within the enclosure.

Similar to experimental, in numerical investigations, also existing constant height fin heat sink and variable height fin heat sink are compared. But during this comparison of heat sinks, the influence of aspect ratio and fin shapes on both enclosures is also briefed. The variable height fin heat sinks provide better thermal performance during melting and solidification under any aspect ratio. Likewise, for any fin shapes, during both cycles, a variable height fin heat sink is a preferable choice over the constant height fin heat sinks. Moreover, the square fin shape can be replaced with the triangular fin shape, which exhibits better enhancement during both cycles.

6. Conclusion

A pin-fin heat sinks with constant height fin height and variable height fin height arrangements were experimentally and numerically investigated. The fins employed in both heat sinks have a constant volume fraction of 8 %. The PCM incorporated in this analysis is n-eicosane. First, experimental analysis was done to obtain a better heat sink configuration among conventional constant height fin heat sinks and modified variable fin height heat sinks. Under constant heat load and power surge heat load, temperature-time histories were evaluated. Based on the outcomes, a comparative interpretation was made in various scenarios.

- The variable height fin heat sink accelerates any load's melting rate. The time difference between the wall and the PCM is also less for the variable height fin heat sink. The reason is that the distribution of fins throughout the enclosure reduces the resistance the PCM offers. This results in a uniform melting and high heat transfer rate within the enclosure.
- Similar to the melting, a faster discharging rate is noticed during solidification in the variable height fin heat sink. But for both heat sinks, there is a disparity between solidification and melting time. When the heat input is increased, the time taken for the heat sink base to reach 30 °C is shortened.

Then, a 3D computational model was developed, and simulations were carried out using ANSYS Fluent 19.0. This numerical simulation discusses the effect of various aspect ratios on both the heat sinks. Additionally, the fin geometry has also been varied, and the influence of shapes on both the heat sinks has been investigated for both cycles.

- In numerical simulations, the contour images give the impact of variable height fin heat sink at any aspect ratio (0.3–0.8). In the top section of the enclosure, the temperature distribution within the PCM is more for variable height fin heat sink, and it accelerates the melting. A decreasing slope of the time difference between the heat sinks is spotted during solidification when the aspect ratio increases.
- Four different shapes, including square, circular, diamond, and triangular, are examined for both cycles. The triangular fin displays a faster melting and solidification rate among these shapes. A high enhancement percentage of 2.29 % for constant height fins and 12.5 % for variable height fins are obtained when triangular fin shapes are incorporated.

Nomenclature

A	mushy zone constant
b	width (mm)
c_p	specific heat (kJ/kg K)
d	diameter (mm)
f	fin
$\vec{g}$	acceleration due to gravity (m/s^2)
H	enthalpy (J/kg)
h	height (mm)
h_f	fin height (mm)
h_{ref}	reference enthalpy (J/kg)
h_s	sensible enthalpy (J/kg)
I	current (amp)
k	thermal conductivity (W/mK)
L	latent heat of fusion (kJ/kg)
l	length (mm)
n	number of fins
P*	pressure (N/m^2)
P	power (W)
PCM	phase change material
PV	photovoltaic
$\dot{q}$	heat flux (W/m^2)
s	fin spacing (mm)
TCE	thermal conductivity enhancer
T	temperature (K)
t	time (s)
T_l	liquidus temperature (K)
T_m	melting temperature of PCM
T_r	reference temperature (K)
T_s	solidus temperature (K)
T_w	wall temperature (K)
u,v,w	velocity in x and y direction (m/s)
V	voltage (volt)
w	base (mm)
x,y,z	spatial coordinates (m)

Greek symbols

ρ	density (kg/m^3)
μ	dynamic viscosity (kg/ms)
β_0	coefficient of thermal expansion (1/K)
Φ	liquid fraction
λ	constant
ω	uncertainty

Subscripts

e	enclosure
HS	heat sink
i	initial
p	PCM
pl	a pitch from the long side of the enclosure
ps	a pitch from the short side of the enclosure
sl	spacing from the long side of the enclosure
ss	spacing from the long side of the enclosure

Declaration of competing interest

We confirm that there is no conflict of interest to be declared.

Data availability

Data will be made available on request.

References

[1] Ç. Yıldız, M. Arıcı, S. Nižetić, A. Shahsavar, Numerical investigation of natural convection behavior of molten PCM in an enclosure having rectangular and tree-like branching fins, Energy 207 (2020), https://doi.org/10.1016/j.energy.2020.118223.

[2] M.S. Mahdi, H.B. Mahood, A.A. Alammar, A.A. Khadom, Numerical investigation of PCM melting using different tube configurations in a shell and tube latent heat thermal storage unit, Therm. Sci. Eng. Prog. 25 (2021), 101030, https://doi.org/10.1016/j.tsep.2021.101030.

[3] M. Selvan, G. Nagarajan, K. Hooman, Numerical analysis of multiple phase change materials based heat sink with angled thermal conductivity enhancer, J. Energy Storage 55 (2022), 105316, https://doi.org/10.1016/j.est.2022.105316.

[4] Y.H. Wang, Y.T. Yang, Three-dimensional transient cooling simulations of a portable electronic device using PCM (phase change materials) in multi-fin heat sink, Energy 36 (2011) 5214–5224, https://doi.org/10.1016/j.energy.2011.06.023.

[5] Q. Ma, Z. Wang, T. Liang, Y. Su, J. Li, Y. Yao, X. Zeng, Y. Pang, M. Han, X. Zeng, J. Xu, L. Ren, R. Sun, Unveiling the role of filler surface energy in enhancing thermal conductivity and mechanical properties of thermal interface materials, Compos. Part A Appl. Sci. Manuf. 157 (2022), 106904, https://doi.org/10.1016/j.compositesa.2022.106904.

[6] M.S. Nedumaran, G. Trilok, N. Gnanasekaran, K. Hooman, Multi-objective optimization of hybrid heat sinks with phase change materials, Heat Transf. Eng. 0 (2023) 1–22, https://doi.org/10.1080/01457632.2023.2234770.

[7] M. Opolot, C. Zhao, M. Liu, S. Mancin, F. Bruno, K. Hooman, Investigation of the effect of thermal resistance on the performance of phase change materials, Int. J. Therm. Sci. 164 (2021), 106852, https://doi.org/10.1016/j.ijthermalsci.2021.106852.

[8] Z.Q. Zhu, Y.K. Huang, N. Hu, Y. Zeng, L.W. Fan, Transient performance of a PCM-based heat sink with a partially filled metal foam: effects of the filling height ratio, Appl. Therm. Eng. 128 (2018) 966–972, https://doi.org/10.1016/j.applthermaleng.2017.09.047.

[9] H. Zheng, C. Wang, Q. Liu, Z. Tian, X. Fan, Thermal performance of copper foam/paraffin composite phase change material, Energy Convers. Manag. 157 (2018) 372–381, https://doi.org/10.1016/j.enconman.2017.12.023.

[10] G.K. Marri, R. Srikanth, C. Balaji, Effect of phase change and ambient temperatures on the thermal performance of a solid-liquid phase change material based heat sinks, J. Energy Storage 30 (2020), 101327, https://doi.org/10.1016/j.est.2020.101327.

[11] N. Raźny, A. Dmitruk, M. Serdechnova, C. Blawert, J. Ludwiczak, K. Naplocha, The performance of thermally conductive tree-like cast aluminum structures in PCM-based storage units, Int. Commun. Heat Mass Transf. 142 (2023), https://doi.org/10.1016/j.icheatmasstransfer.2022.106606.

[12] T. Bouzennada, F. Mechighel, T. Ismail, L. Kolsi, K. Ghachem, Heat transfer and fluid flow in a PCM-filled enclosure: effect of inclination angle and mid-separation fin, Int. Commun. Heat Mass Transf. 124 (2021), 105280, https://doi.org/10.1016/j.icheatmasstransfer.2021.105280.

[13] M.O. Karaağaç, A. Ergün, Ü. Ağbulut, A.E. Gürel, İ. Ceylan, Experimental analysis of CPV/T solar dryer with nano-enhanced PCM and prediction of drying parameters using ANN and SVM algorithms, Sol. Energy 218 (2021) 57–67, https://doi.org/10.1016/j.solener.2021.02.028.

[14] R. Elarem, T. Alqahtani, S. Mellouli, W. Aich, N. Ben Khedher, L. Kolsi, A. Jemni, Numerical study of an evacuated tube solar collector incorporating a nano-PCM as a latent heat storage system, Case Stud. Therm. Eng. 24 (2021), 100859, https://doi.org/10.1016/j.csite.2021.100859.

[15] M. Moein-Jahromi, H. Rahmanian-Koushkaki, S. Rahmanian, S. Pilban Jahromi, Evaluation of nanostructured GNP and CuO compositions in PCM-based heat sinks for photovoltaic systems, J. Energy Storage 53 (2022), 105240, https://doi.org/10.1016/j.est.2022.105240.

[16] M.A. Abdelkareem, H.M. Maghrabie, A.G. Abo-Khalil, O.H.K. Adhari, E.T. Sayed, A. Radwan, H. Rezk, H. Jouhara, A.G. Olabi, Thermal Management Systems Based on Heat Pipes for Batteries in EVs/HEVs, Elsevier Ltd, 2022, https://doi.org/10.1016/j.est.2022.104384.

[17] W.N. Septiadi, M. Alim, M.N.P. Adi, The application of battery thermal management system based on heat pipes and phase change materials in the electric bike, J. Energy Storage 56 (2022), 106014, https://doi.org/10.1016/j.est.2022.106014.

[18] A.H. Mosaffa, F. Talati, H. Basirat Tabrizi, M.A. Rosen, Analytical modeling of PCM solidification in a shell and tube finned thermal storage for air conditioning systems, Energy Build. 49 (2012) 356–361, https://doi.org/10.1016/j.enbuild.2012.02.053.

[19] T. Bouhal, Z. Meghari, S. ed D. Fertahi, T. El Rhafiki, T. Kousksou, A. Jamil, E. Ben Ghoulam, Parametric CFD analysis and impact of PCM intrinsic parameters on melting process inside enclosure integrating fins: solar building applications, J. Build. Eng. 20 (2018) 634–646, https://doi.org/10.1016/j.jobe.2018.09.016.

[20] Z. Elmaazouzi, I.A. Laasri, A. Gounni, M. El Alami, A. Outzourhit, E.G. Bennouna, Coupled parameters evaluation of three different finned structures for concentrated solar thermal energy storage, J. Energy Storage 51 (2022), 104523, https://doi.org/10.1016/j.est.2022.104523.

[21] S. Khanna, K.S. Reddy, T.K. Mallick, Optimization of finned solar photovoltaic phase change material (finned pv pcm) system, Int. J. Therm. Sci. 130 (2018) 313–322, https://doi.org/10.1016/j.ijthermalsci.2018.04.033.

[22] Z. Sun, R. Fan, F. Yan, T. Zhou, N. Zheng, Thermal management of the lithium-ion battery by the composite PCM-fin structures, Int. J. Heat Mass Transf. 145 (2019), 118739, https://doi.org/10.1016/j.ijheatmasstransfer.2019.118739.

[23] F. Liu, J. Wang, Y. Liu, F. Wang, Y. Chen, Q. Du, F. Sun, N. Yang, Natural convection characteristics of honeycomb fin with different hole cells for battery phase-change material cooling systems, J. Energy Storage 51 (2022), 104578, https://doi.org/10.1016/j.est.2022.104578.
[24] A.N. Desai, A. Gunjal, V.K. Singh, Numerical investigations of fin efficacy for phase change material (PCM) based thermal control module, Int. J. Heat Mass Transf. 147 (2020), 118855, https://doi.org/10.1016/j.ijheatmasstransfer.2019.118855.
[25] C.S. Miers, A. Marconnet, Experimental investigation of composite phase change material heat sinks for enhanced passive thermal management, J. Heat Transf. 143 (2021) 10–12, https://doi.org/10.1115/1.4048620.
[26] M.R. Singh, A. Giri, A comparison of the performance of constant and dual height pin fins in phase change material cooling technique, J. Therm. Sci. Eng. Appl. 13 (2021) 1–11, https://doi.org/10.1115/1.4048665.
[27] H.M. Ali, A. Arshad, M. Jabbal, P.G. Verdin, Thermal management of electronics devices with PCMs filled pin-fin heat sinks: a comparison, Int. J. Heat Mass Transf. 117 (2018) 1199–1204, https://doi.org/10.1016/j.ijheatmasstransfer.2017.10.065.
[28] A.N. Desai, H. Shah, V.K. Singh, Novel inverted fin configurations for enhancing the thermal performance of PCM based thermal control unit: a numerical study, Appl. Therm. Eng. 195 (2021), 117155, https://doi.org/10.1016/j.applthermaleng.2021.117155.
[29] C. Ji, Z. Qin, S. Dubey, F.H. Choo, F. Duan, Simulation on PCM melting enhancement with double-fin length arrangements in a rectangular enclosure induced by natural convection, Int. J. Heat Mass Transf. 127 (2018) 255–265, https://doi.org/10.1016/j.ijheatmasstransfer.2018.07.118.
[30] R. Akula, C. Balaji, Thermal performance of a phase change material-based heat sink subject to constant and power surge heat loads: a numerical study, J. Therm. Sci. Eng. Appl. 13 (2021) 1–13, https://doi.org/10.1115/1.4047944.
[31] X.H. Yang, S.C. Tan, Y.J. Ding, L. Wang, J. Liu, Y.X. Zhou, Experimental and numerical investigation of low melting point metal based PCM heat sink with internal fins, Int. Commun. Heat Mass Transf. 87 (2017) 118–124, https://doi.org/10.1016/j.icheatmasstransfer.2017.07.001.
[32] S. Shaikh, K. Lafdi, C/C composite, carbon nanotube and paraffin wax hybrid systems for the thermal control of pulsed power in electronics, Carbon N. Y. 48 (2010) 813–824, https://doi.org/10.1016/j.carbon.2009.10.034.
[33] L.W. Fan, Z.Q. Zhu, Y. Zeng, Y.Q. Xiao, X.L. Liu, Y.Y. Wu, Q. Ding, Z.T. Yu, K. F. Cen, Transient performance of a PCM-based heat sink with high aspect-ratio carbon nanofillers, Appl. Therm. Eng. 75 (2015) 532–540, https://doi.org/10.1016/j.applthermaleng.2014.10.050.
[34] M. Taghilou, E. Khavasi, Thermal behavior of a PCM filled heat sink: the contrast between ambient heat convection and heat thermal storage, Appl. Therm. Eng. 174 (2020), 115273, https://doi.org/10.1016/j.applthermaleng.2020.115273.
[35] W.B. Ye, Thermal and hydraulic performance of natural convection in a rectangular storage cavity, Appl. Therm. Eng. 93 (2016) 1114–1123, https://doi.org/10.1016/j.applthermaleng.2015.10.083.
[36] X. Yang, X. Wang, Z. Liu, Z. Guo, K. Hooman, Thermal performance assessment of a thermal energy storage tank: effect of aspect ratio and tilted angle, Int. J. Energy Res. 45 (2021) 11157–11178, https://doi.org/10.1002/er.6598.
[37] A. Samimi Behbahan, A. Noghrehabadi, C.P. Wong, I. Pop, M. Behbahani-Nejad, Investigation of enclosure aspect ratio effects on melting heat transfer characteristics of metal foam/phase change material composites, Int. J. Numer. Methods Heat Fluid Flow 29 (2019) 2994–3011, https://doi.org/10.1108/HFF-11-2018-0659.
[38] M. Choi, K. Cho, Effect of the aspect ratio of rectangular channels on the heat transfer and hydrodynamics of paraffin slurry flow, Int. J. Heat Mass Transf. 44 (2001) 55–61, https://doi.org/10.1016/S0017-9310(00)00095-8.
[39] Y. Zhang, Z. Rao, S. Wang, Z. Zhang, X. Li, Experimental evaluation on natural convection heat transfer of microencapsulated phase change materials slurry in a rectangular heat storage tank, Energy Convers. Manag. 59 (2012) 33–39, https://doi.org/10.1016/j.enconman.2012.02.004.
[40] S.K. Saha, K. Srinivasan, P. Dutta, Studies on optimum distribution of fins in heat sinks filled with phase change materials, J. Heat Transf. 130 (2008) 1–4, https://doi.org/10.1115/1.2804948.
[41] M.S. Nedumaran, N. Gnanasekaran, Comprehensive analysis of hybrid heat sinks with phase change materials for both charging and discharging cycles, Heat Transf. Eng. 0 (2022) 1–19, https://doi.org/10.1080/01457632.2022.2059216.
[42] ANSYS Inc., ANSYS Fluent Software Package v19.5, (n.d.). https://www.afs.enea.it/project/neptunius/docs/fluent/html/ug/main_pre.htm.
[43] M. Parsazadeh, X. Duan, Numerical and experimental investigation of phase change heat transfer in the presence of Rayleigh–Benard convection, J. Heat Transf. 142 (2020) 1–13, https://doi.org/10.1115/1.4046537.
[44] D. Yoo, Y. Joshi, Energy efficient thermal management of electronic components using solid liquid phase change materials, in: Intersoc. Conf. Therm. Thermomechanical Phenom. Electron. Syst. ITHERM. 2002-Janua, 2002, pp. 800–807, https://doi.org/10.1109/ITHERM.2002.1012536.